Giampiero Amato, Gianluca Milano, Umberto Vignolo, Ettore Vittone. Kinetics of defect formation in chemically vapor deposited (CVD) graphene during laser irradiation: The case of Raman investigation. NANO RESEARCH. 8 (12) pp: 3972-3981.
DOI: 10.1007/s12274-015-0900-1

Kinetics of defects formation in CVD graphene during Laser irradiation: the case of Raman investigation

Giampiero Amato[1], Gianluca Milano[2], Umberto Vignolo[2] and Ettore Vittone[2]♦

[1]Quantum Research Laboratory, INRIM, Strada delle Cacce 91, Torino, Italy

[2] Department of Physics, University of Torino, via Pietro Giuria 1, 10125 Torino, Italy

ABSTRACT

The effects of laser irradiation on Chemically Vapor Deposited graphene is studied by analyzing the temporal evolution of Raman spectra acquired under different illumination conditions. It is observed that the normalized intensity of the defect-related peak increases with the square root of the time of exposure, in a nearly linear way with the laser power density and that the hardness of graphene to the radiation damage depends on its intrinsic structural quality. The results suggest that, contrarily to the common belief, micro-Raman cannot be considered as a non-invasive tool for characterization of graphene.

The experimental observation are compatible with a model, we have derived from the interpretative approach of the Staebler-Wronski effect in hydrogenated amorphous silicon, which assumes that photoexcited carrier recombination induces the breaking of weak C-C bonds.

KEYWORDS

CVD graphene, Raman spectroscopy, Defect kinetics, Laser irradiation

♦ Correponding author: Ettore Vittone, e-mail: vittone@to.infn.it

1. Introduction

Metastability of thin films grown either by physical or chemical vapor deposition, has been extensively observed in last decades as a variety of phenomena occurring in numerous materials. Examples can be mentioned like structural changes produced by heating, e.g, agglomeration [1] or the creation of additional defects under electrical or optical stimulation [2].

A phenomenological description of this class of systems considers the configurational ground state as not given by an absolute and isolated minimum of the total potential energy, but rather by a more flexible arrangement of the atoms allowing configurations with different local minima of the potential energy separated by a more or less continuous distribution of barriers. In the case of two configurational energy minima with energy difference ΔE, and separated by a barrier of height V_0, if the externally applied excitation is $E_{ex} \geq \Delta E + V_0$, stimulated transitions between the two configurational states become possible, or, if the barrier is thin enough, transition between minima can spontaneously occur by tunneling. A class of phenomena, occurring in both crystalline and amorphous solids, is observed under non-thermal-equilibrium conditions, for example, during illumination which, in some cases, degrades the material properties, whereas a relaxation into the equilibrium ground state and a recovery of its properties is possible, e.g. by annealing [2].

There are, in literature, reports about the healing, or self-healing of graphene defects. Those papers are generally dealing with the employment of thermal treatments [3], aided by the presence of loose C atoms and/or catalyzing metal atoms [4], or by atomic layer deposition of metals [5] or Al_xO_y compounds [6] and their results suggest that the metastability of defects can be encountered also in graphene. This either opens an additional route for improving the properties of the material grown by

Chemical Vapor Deposition (CVD) with the aim of large-area production of graphene crystals, or allows for tailoring of its properties in a bottom-up fashion. The mechanism can however be studied in the opposite way, for example, by intentionally producing defects, and by following their formation kinetics.

Raman spectroscopy is considered as one of the best tools to assess the quality and the structural properties of graphene [7,8]. The features contained in a typical Raman spectrum of graphene can be distinguished in the following way: the first observable peak appears at ≈1590 cm^{-1} and is associated with the zone-center in-plane longitudinal optical phonons. This well-known *G* peak is characteristic for sp^2-hybridized carbon-carbon bonds. The second prominent peak is located at ≈2700 cm^{-1}. This 2*D* peak originates from a double-resonance process, which creates an electron-hole pair that recombine after two inelastic-scattering events involving phonons with opposite momenta. If defects are present, one of the two scattering events can occur elastically and the *D* peak, observed in this case, exhibits only half the Raman shift. With intense *D* peaks, a concomitant drop in the intensity of the 2*D* peak is observed.

Both the wealth of information contained in Raman spectra, and its, in principle, non-destructive character (no sample preparation is required, photons are employed) make this technique one of the routine characterization tool to characterize graphene and to optimize its synthesis [9]. However, there are evidences in literature about the modification of graphene properties induced by intense laser irradiation, either in terms of reversible photon-induced doping of the material [10], disassembly of graphene monocrystal into a nanocrystalline network [11]**,** or ablation of graphene multilayer till to a monolayer [12,13].

For these reasons, when the laser light is focused down to the diffraction limit, as in micro-Raman instruments, possible sample damage can occur, as reported in the case of exfoliated material [11]. The assessment of the technique in the case of CVD graphene is then necessary, otherwise information

extracted on the samples quality cannot be reliable at all.

This paper describes experiments carried out on CVD graphene samples aimed to investigate the effects of laser irradiation and intend to propose a model able to interpret the kinetics of defect evolution in terms of illumination time and laser power density.

2. Experimental

The synthesis of graphene was performed by CVD, using a 99.8% Cu foil (Alpha Aesar N°13382) as a catalyst and CH_4 as precursor gas in a vacuum chamber of a Rapid Thermal Annealing apparatus [13]. The Cu foil was initially cleaned with acetic acid at 60°C, sonicated in acetone and ethanol and then inserted in the reactor chamber, encapsulated in between two oxidized silicon wafers. The encapsulation of the Cu foil produces a closed environment, which increases the quality of graphene, by promoting a lower number of nucleation centers and, consequently, larger graphene domains [14]. After a first step of 5 minutes in H_2 atmosphere to remove residual Cu oxide, 30 sccm of CH_4 and 20 sccm of H_2 were introduced in the chamber for 5 minutes at constant temperature of 1025 °C and pressure of 6.7 mbar. The obtained graphene was then transferred on a Si substrate with 300 nm SiO_2, using PMMA as a supporting layer [15]. The graphene layer on the back-side of the Cu foil was etched with O_2 plasma, before dipping the sample in a 1M $FeCl_3$ solution for Cu removal. After several washing steps in H_2O, PMMA/graphene structure was picked up with the Si/SiO_2 target substrate with Au/Pd markers that were prefabricated by optical lithography. PMMA was removed by acetone.

The apparatus for Micro-Raman analysis was composed of a Diode Pumped Solid State Laser at λ=532 nm and 150 mW power. Spurious components of the laser line were filtered by an Omega Optical interference filter centered at 532 nm. A beam-splitter with 98% transmission at 45°, from Omega Optical was placed in a Leitz Secolux 6x6 microscope and directed the laser onto a 125x, 0.80

n.a. microscope objective. The spot was focused to a diameter d=2 μm, instead of 1 μm, to reduce the power density. Sample was moved by means of two mechanical stages from Physik Instrumente with resolution of 124 steps/μm. Emitted light was filtered by means of a Sciencetech 9030DS Double Subtractive Monochromator, and analyzed by a Solar Laser Systems M833 Double Monochromator, equipped with two 600 l/mm gratings. Spectra were recorded by a Hamamatsu C7040 back-thinned CCD head. All the system was controlled by a software developed under LabView™.

3. Results and discussion

Fig. 1a shows the Raman spectrum of the CVD graphene, collected in macro- configuration with a laser (λ=532 nm, wavelength) spot of d=100 μm diameter and a laser power at the sample P=11.7 mW (power density, $\Psi \approx 150$ W/cm^2) for T_{integ}=60 s integration time. The spectrum is compared with a typical one from micro-Raman of exfoliated graphene [11], to highlight the similar quality, apart from the slightly higher *D* peak in the CVD case. Considering the spatial averaging character of the macro-tool, this encouraging result suggested us to perform micro-Raman investigation to select the best areas, which reasonably should show an even better quality.

Quite surprisingly, most of the micro-Raman spectra collected in a standard configuration (λ=532 nm, d=2 μm, P=2 mW, $\Psi \approx 6.4 \cdot 10^4$ W/cm^2, T_{integ}=45 s), show a *D* peak more pronounced than the macro-case. The spectrum resulting from mathematical averaging of ~1400 acquisitions collected by the micro- tool on a 40x30 μm^2 area shows a more pronounced *D* peak, related to defects, than the corresponding macro- one, as evidenced in Fig. 1b. According to Krauss et al. [11], these preliminary results indicate that additional defects are created when focusing the laser down to a micrometer-sized spot. It seems, in addition, that the application of the Raman technique to CVD graphene (instead of exfoliated), is harmful to the sample, despite the employment of lower power (64 kW/cm^2 against [11]

400 kW/cm^2) and energy (3.8 MJ/cm^2 against [11] 12 MJ/cm^2) densities. Actually, Tiberj et al. [10] reported about photo-induced doping as directly connected to the substrate preparation, evidencing that, when graphene is transferred onto Si/SiO_2 substrates used as-received and without any cleaning, the doping of graphene flakes remains constant for all the entire laser power range. Doping from adsorbates has to be considered as an alternative origin for spectral changes in Raman spectra, the most evident being the blue-shift of the *G* band [11,16]. Raman *G-mode* softening and shifting with illumination time have been observed by Krauss et al. [11] and ascribed to laser heating as presumably responsible for the dopant removal. In all our experiments, however, we did not observe any variation in the intensity and position of the Raman *G-mode*, both with time and illumination power density, as discussed in the following. This confirms the conclusions of Tiberj et al. [10], since we transferred graphene onto as-received substrates, and suggests a negligible amount of adsorbates onto the graphene surface.

In order to elucidate the effect of the degradation of graphene quality induced by laser irradiation, we performed micro-Raman spectroscopy studies using different laser power densities, which have been reduced to 50% (Ψ = 32 kW/cm^2), 80% (51 kW/cm^2), and 90% (58 kW/cm^2) by means of neutral density filters.

Fig. 2 shows maps of the I_D/I_G Raman peak intensity ratio from two graphene regions (16 μm x 16 μm): maps a) and b) are collected in the first region at power levels increasing from 80% to 100%, and d) and e) in the second one at power levels decreasing from 100% and 80%, respectively. The acquisition time for each point was T_{Integ}=45 s. The differential maps displayed in c) and f) evidence the different damaging effects of the second exposure. The role played by the laser power in the formation of additional defects is evident, since the damage induced by the second exposure is higher in the case of increasing power level (first region). However, both cases show that defective graphene is more prone to further degradation. This indirectly agrees with the results of Krauss et al. [11], who

needed to employ one order of magnitude higher power density to produce defects in exfoliated graphene, where the Raman *D* mode is generally very weak, indicating a low concentration of pristine defects.

CVD graphene is polycrystalline, being formed of grains with characteristic dimensions ranging from tens of nm up to hundreds of μm, depending on the deposition conditions. Raman spectroscopy is often employed to estimate the average grain dimension, which correlates well with the I_D/I_G intensity ratio [17]. This reasoning bases on the observation that most of the defects are located at grain boundaries.

There is another Raman feature, the *D'* peak, located at ≈1600 cm^{-1}, and ascribed to states lying at the zigzag boundaries, whereas the *D* peak, is associated to armchair boundaries [17]. In all our investigations, however, the *D'* peak has never been observed, suggesting a higher formation energy for this kind of defects. This is in agreement with theoretical calculations of formation energy of armchair and zigzag boundaries in graphene nano-ribbons [18] Actually, it is found that the formation of armchair boundaries requires an energy about 2.3 eV per atom, 1 eV per atom less than the case of zigzag boundaries. This is due to substantial lattice relaxation which takes place on the armchair edge, with a bond length of the edge C atoms of 0.123 nm. In contrast, the lattice relaxation at the edge atomic site does not take place for the zigzag edges and a bond length of 0.138 nm is calculated. A similar situation could be envisaged in the case of topological defects, say, pentagons, where the formation of armchair-related defects would require a smaller energy. It is worth noting that the formation energy of armchair edges is not too far from the energy of impinging photons in a conventional Raman apparatus employing green light, and, consequently, to the energy released to the lattice by non-radiative recombination of a photo generated electron-hole pair.

A systematic analysis of defect evolution with time by employing different laser energies can provide a deeper insight into the nature of these metastable defects. However, this study is beyond the scope of

this work, which is focused on the analysis of the kinetics of these defects during laser irradiation

The distribution of the I_D/I_G intensity ratios extracted from a Raman map is asymmetrical and well described by a log-normal function as shown in Fig. 3. Here, two distributions, arising from maps collected at two power densities (80% and 100%, respectively) onto two different, but adjacent areas, are displayed. Increasing the laser power results in a broader distribution shifted towards higher values of I_D/I_G. On the other hand, it is worth noticing that the I_{2D}/I_G intensity ratio is always symmetrically distributed.

A log-normal distribution is the result of a process in which a variate obeys the law of proportionate effect, i.e. the change of the variate at any step of the process is a random proportion of the previous value of the variate [19]. Therefore, the random evolution of the I_D/I_G ratio, induced by laser irradiation, can be expressed as a percentage of the number of defects, with a proportionality factor depending on the laser power. This indirectly corroborates the evidence that defects existing in pristine material act as seeds for propagating laser induced ones.

In order to study the kinetics of defect formation in CVD graphene we have analysed the evolution of the Raman spectra obtained by focusing the laser (Ψ=64 kW/cm^2, d=2 μm,) onto three points of the sample, which showed similar pristine I_D/I_G ratio but different I_{2D}/I_G. The laser irradiated these points for 2 hours and spectra were acquired at fixed intervals of 10 min with integration time of T_{Integ}=45 s. The I_D/I_G intensity ratio is found to monotonically increase with the square root of time. Fig. 4a shows a typical trend.

This dependence suggests that the rate of formation of new defects is higher at the first stage of illumination, and gradually decreases. All the investigated spots on the sample surface display this $K \cdot t^{1/2}$ dependence, but with different values of the proportionality factor K, indicating a different reactivity to the damaging action of the laser beam. Maps in Fig. 2 suggest that such reactivity is strongly reduced in regions where pristine defects are absent, meaning that K≈0, there. This

observation is corroborated by Fig. 4a, in which the slopes of the linear fits (in the $t^{1/2}$ scale) increase with the value of the initial I_D/I_G peak ratio.

We found additional dependence of the K slope on the I_{2D}/I_G intensity ratio. In Fig. 4a, data relevant to regions with $I_{2D}/I_G \approx 4$, show different slopes (vs. $t^{1/2}$) because of the different initial defect concentrations. However, their linear behaviors are remarkably steeper than the linear trend of data relevant to $I_{2D}/I_G = 2$. This evidence suggests that samples with larger I_{2D}/I_G ratios are generally more prone to photon damage, or, in other words, that bilayer graphene is more laser radiation hard. Furthermore, the proportional factor K is function of the power density Ψ. This fact is evidenced by the I_D/I_G time evolution resulting from the illumination of the same spot of the sample at successive different power levels (namely 50%, 80%, 90%, and 100%) for the same time interval, obtaining this way the data displayed in Fig 4b. Here the colored bar chart refer to the right axis and indicates the different powers, whereas the quantity I_D/I_G (left axis) is plotted against the square root of time for the four cycles, evidencing the change in slope due to different Ψ values.

To summarize, our experiments provide evidence that the density of defects induced by laser irradiation follows a general behavior, which appears in Raman spectroscopy through the dependence on the I_D/I_G ratio:

i) On the initial values of the defect density in pristine conditions.

ii) On the square root of the time exposure at fixed laser power density.

iii) On the electron-hole pair photogeneration rate G (which is proportional to the power density Ψ) in a nearly linear way.

A thermal mechanism, related to the sample heating at the laser spot, could be envisaged to explain the photo-induced formation of defect. The well-defined dependence, summarized above, of the I_D/I_G ratio on the experimental parameters is however difficult to explain in the framework of a simple thermal model. Actually, sample heating can be monitored through the spectral evolution of the

Raman modes (the *G* peak above all), with time and power density [20]. As displayed in Fig. 5, no appreciable shift is observed for such feature either with time or with laser intensity, suggesting a temperature rise on the light spot of some tens °C [20]. Basing on these consideration, the thermal origin for the defect creation can be ruled out.

All the experimental findings can be included in the following expression instead:

$$N_d(t_{ill}) - N_d(0) = const \cdot G^{\kappa} \cdot t_{ill}^{1/2} \qquad (1)$$

where it is assumed that the density of defects $N_d(t_{ill})$ is proportional to the I_D/I_G intensity ratio, t_{ill} is the laser exposure time, $N_d(0)$ is the pristine defect density, and the constant is actually position-dependent. According to eq. (1), the results of the fits in Fig. 4b can be plotted against Ψ, by considering the photogeneration rate G as proportional to the laser power density Ψ (see point iii). The inset shows that a power law with exponent κ close to unity (1.0±0.2) could be envisaged, albeit with a relatively large uncertainty, as after-effect of the indirect nature of the measurement. It has to be noticed, however, that illumination cycles repeated on other sample spots yielded approximately the same power law. Consequently, eq. (1) can be considered as descriptive of the kinetics of defect formation in CVD graphene under intense illumination and suggests a lack of reciprocity between intensity and time. Actually, doubling the integration time and halving the laser power during a Raman measurement is not equivalent to the opposite in terms of laser-induced disassembly of graphene. According to eq. (1), the first approach seems less detrimental to the sample's quality, meaning that employing lower power densities is a safer strategy. In order to investigate if there is a safety limit to the power density value, we reduced it down to the lowest limit for our apparatus, Ψ=19 kW/cm^2, with T_{integ}=600 s, in order to yield spectra with acceptable S/N ratio. These conditions are obviously unpractical for acquiring Raman maps, but allow following the time evolution of defects on a single spot. We observed an increase for the I_D/I_G intensity ratio of 30% for the first 120 min of illumination,

with the same trend of eq. (1). Possible departures from this trend could be observed with Raman instruments with superior optical quality employing lower laser power levels or by excitation with less energetic photons. In this case, however, the scaling of the Raman cross section with the inverse fourth power of the excitation photon energy, requires, in principle, longer integration times.

Eq. (1) is reminiscent of a relationship proposed by Stutzmann et al. [2] to explain the kinetics of transition of metastable defects occurring in hydrogenated amorphous silicon (a-Si:H) under illumination, the so-called Staebler-Wronski effect.

There are, however, important differences: in the a-Si:H case the power law of defect evolution is cubic, and not quadratic as in eq. (1); differently from our case, in that model $N_d(0) << N_d(t_{ill})$ and is generally negligible; last, the relationship from Stutzmann et al. [2] is a simplified version of a more complex model, and is obtained for low injection rates.

The recombination, if non-radiative, provides the energy necessary for breaking the associated weak bonds. Then, the process involved is the electron-hole recombination at band-tail states, which are metastable defects related to weak (elongated, distorted) bonds of the a-Si:H network.

The last argument can be extended to the case of CVD graphene, considering its polycrystalline nature. Defects in graphene are known to be spatially located mainly at grain boundaries, where it is reasonable that covalent bonds of neighboring C atoms are weaker: one C atom on the border shows only two, reasonably weaker, saturated bonds, whereas pentagons, or heptagons are more likely to be present [4]. Then, the density of weaker, metastable bonds (WB) is reasonably higher in proximity of pre-existing defects. This argument simply explains the observation that CVD graphene is more prone to laser damage than exfoliated one, and different portions of the same sample are resistant to the laser damage in different fashions.

There is a general agreement about the enhancement of the *D* mode and the concurrent softening of the *2D* mode in highly defective graphene [11]. We argue that Raman scattering at metastable bonds

occurs through the *2D* transition, and involves two photons with energy *ħΩ'*, which is in principle different from the phonon energy *ħΩ, e*xchanged in the *2D* Raman scattering at stable bonds. By analogy with the case of folded graphene, where the Fermi velocity is lowered by a few percent [16]**,** such reduction can also occur in the case of elongated/distorted bonds. This means that Dirac's cones are somewhat broadened at those sites. Moreover, there are theoretical studies showing how breaking of the honeycomb symmetry can lead to distorted Dirac's cones, as in the case of Graphynes [21-22]. It can be noted, in passing, that a larger distortion of the Dirac's cone on defect sites has been proposed to keep into account for the elastic scattering, which is at the origin of the *D* mode [23].

The occurrence of *2D* transitions at distorted Dirac's cones, with different exchanged phonon energies, is in agreement with the observation that in defective regions the *2D* mode is generally broader. Then, Raman technique allows the monitoring of defect evolution as a balance between *D* and *2D* transitions. Defects creation tends to enhance the *D* mode, and to shunt the *2D* transition, by opening additional electron-hole recombination pathways through photogenerated defects. Actually, Fig. 6 displays the correlation between the *D* and *2D* peak intensities obtained on different portions of the graphene sample at two different laser powers, evidencing that photogeneration of defects reduces the intensity of the competitive *2D* transitions. This explains the self-limiting trend of the defect formation by photogeneration.

The above argument can be invoked to explain the better stability of bilayer graphene, as evidenced in Fig. 4. It is well known, in fact, that the *2D* structure in bilayer graphene is more complex, being the convolution of 4 different peaks, originating from 4 transitions occurring through the energy sub-bands of such system. Then, more pathways are available for electron-hole recombination. The weight of a specific recombination process responsible for bond-breaking is then reduced.

In order to elaborate a simplified interpretative model of the kinetics of metastable defect creation,

partially borrowed by Stutzmann et al. [2], let us consider the basic set of equations describing generation/recombination phenomena in graphene:

$$\frac{dn}{dt} = G - \beta \cdot n \cdot p - \alpha_n \cdot n \cdot N_d, \quad (2a)$$

$$\frac{dp}{dt} = G - \beta \cdot n \cdot p - \alpha_p \cdot p \cdot N_d, \quad (2b)$$

$$\frac{dN_d}{dt} = \gamma \cdot n_{WB} \cdot p. \quad (2c)$$

n,p are the electron,hole concentrations in the conduction and valence band, respectively. Assuming that the material is nearly intrinsic, at the illumination levels of the experiment *n* and *p* represent the photo-generated electron and hole concentrations, respectively, being $p>>p_0$ and $n>>n_0$, where the subscript "*0*" indicates the carrier concentration in dark conditions and in pristine material. β accounts for the direct band to band recombination and $\alpha_{n,p}$ are the probabilities of recombination transitions in centers relevant to defects with density N_d. Equation (2c) accounts for the creation of new defects by the interaction of a small fraction of electrons in the conduction band (with density n_{WB}) with metastable and weak bonds.

The complete solution of the set of equations (2) is beyond the scope of this work; however, some approximations can be adopted to interpret our experiments. First, we can assume that the increase of defects density is a very slow process with respect to the carrier kinetics, occurring in a much longer time scale than the carrier generation/recombination processes. In this case, eqs. (2a,b) can be solved separately from the equation involving the defect kinetics (eq. 2c). Therefore, the quasi-steady state approach (i.e. *dp/dt=0* and *dn/dt=0*), leads to the following coupled expressions for *n* and *p*:

$$\begin{cases} n = \frac{G}{\beta \cdot p + \alpha_n \cdot N_d} \\ p = \frac{G}{\beta \cdot n + \alpha_p \cdot N_d} \end{cases} \quad (3)$$

At the illuminating time scale, we can account for the evolution of defects by assuming that n_{WB}

electrons undergo a pure monomolecular recombination:

$$\frac{dn_{WB}}{dt_{ill}} \approx \frac{d}{dt_{ill}}\left[\frac{G}{\alpha_n \cdot N_d}\right] = -\frac{G}{\alpha_n}\left[\frac{1}{N_d}\right]^2 \cdot \frac{dN_d}{dt_{ill}} \quad . \tag{4}$$

By inserting eqs. (4) in eq. (2c), we obtain:

$$\frac{d^2 N_d}{dt_{ill}^{\ 2}} = \gamma \cdot \frac{dn_{WB}}{dt_{ill}} \cdot p \approx -\gamma \cdot p \cdot \frac{G}{\alpha_n} \cdot \left[\frac{1}{N_d}\right]^2 \cdot \frac{dN_d}{dt_{ill}} \quad . \tag{5}$$

The solution of this equation is

$$[N_d(t_{ill})]^2 - [N_d(0)]^2 = 2 \cdot \gamma \cdot p \cdot \frac{G}{\alpha_n} \cdot t_{ill} \quad . \tag{6}$$

For high injection level, i.e. assuming

$$G \gg \frac{\alpha_n \cdot \alpha_p}{\beta} \cdot (N_d)^2 \tag{7}$$

a pure *n-p* bimolecular transition occurs and the hole concentration in the valence band is given by the following expression:

$$p \approx \left(\frac{\alpha_n}{\alpha_p \cdot \beta} G\right)^{\frac{1}{2}}. \tag{8}$$

Finally, by inserting eq. (8) in eq. (6), we obtain:

$$[N_d(t_{ill})]^2 - [N_d(0)]^2 = 2 \cdot \gamma \cdot \left(\frac{G^3}{\alpha_p \cdot \alpha_n \cdot \beta}\right)^{1/2} \cdot t_{ill} \tag{9}$$

Although based on simplified hypotheses, eq. (9) justifies the phenomenological expression given by eq. (1) and gives the time evolution of degradation of metastable bonds into defects N_d. Of course, the formation of new defects leads to the formation of new weak bonds at neighboring sites, leading to a progressive disassembly of the graphene sheets [11].

The derivation of eq. (9) resembles the approach adopted by Stutzmann et al. [2] to model the SW effect in the low illumination condition. However, it is worth to underline that our model is based on the assumption of high injection conditions, defined by eq. (7), which determines a dominant

bimolecular recombination and, consequently, an almost constant hole concentration (eq. 8). This accounts for the $G^{3/4}$ dependence in eq. (9), which is not far from the estimation of κ, as calculated from the fit in Fig. 4(b). On the other hand, the time evolution of defects is assumed to be exclusively determined by a small fraction of photogenerated electrons $n_{WB}<<n$, which undergo a pure monomolecular recombination mediated by defects.

4. Conclusions

In conclusion, a model for the kinetics of defect formation in CVD graphene under illumination is proposed. The model assumes that electron-hole recombination involving weak bonds can provide enough energy to convert metastable bonds into defects and well describes the experimental observations. The kinetics is self-limiting, confirming that the *D* and *2D* are competing transitions for carrier recombination. From a more applicative point of view, it is shown that irregularities in the graphene atomic network make it prone to be damaged by photons, i.e. damaging the mechanically exfoliated material requires a photon flux one order of magnitude larger than CVD. For this reason, great care must be employed when performing Raman characterization of CVD graphene. In particular, there is no reversibility between the time of spectrum integration and the laser power. It is then advisable to reduce the latter, eventually increasing the former. Last, the technique can be fruitfully employed for graphene structuring, taking advantage from the possibility of monitoring *in situ* the evolution of the process.

References

[1] Thompson, C.V. Solid-state dewetting of thin films, *Ann. Rev. of Mat. Res.* **2012**, 42, 399-434.

[2] Stutzmann, M.; Jackson, W.B.; Tsai, C.C. Light-induced metastable defects in hydrogenated

amorphous silicon: A systematic study, *Phys. Rev. B* **1985,** 32, 23–47.

[3] Banhart, F.; Kotakoski, J.; Krasheninnikov, A.V. Structural Defects in Graphene, *ACS Nano* , **2011**, 5, 26–41.

[4] Zan, R.; Ramasse, Q.M.; Bangert, U.; Novoselov, K.S. Graphene Reknits Its Holes, *Nano Lett.;* **2012**, 12, 3936–3940.

[5] Kim K.; Lee H.-B.-R.; Johnson R. W.; Tanskanen J.T.; Liu N.; Kim M.-G.; Pang C.A.; Bent S.F.; Bao Z. Selective metal deposition at graphene line defects by atomic layer deposition, *Nature Communications* **2014**, 5, 4781.

[6] Lam D.V.; Kim S.M.; Cho Y.; Kim J.-H.; Lee H.J.; Yang J.-M.; Lee S.-M.; Healing defective CVD-graphene through vapour phase treatment, *Nanoscale*, **2014**, 6, 5639–5644.

[7] Ferrari, A. C.; Basco, D. M. Raman spectroscopy as a versatile tool for studying the properties of graphene, *Nature Nanotechnology*, **2013**, 8, 235-246.

[8] Jorio, A.; Dresselhaus, M.S.; Saito, R.; Dresselhaus, G. *Raman Spectroscopy in Graphene Related Systems*, John Wiley & Sons. **2011**.

[9] Zhenhua Ni; Yingying Wang; Ting Yu; Zexiang Shen Raman Spectroscopy and Imaging of Graphene, *Nano Res.* **2008**, 1, 273-291.

[10] Tiberj, A.; Rubio-Roy, M.; Paillet, M.; Huntzinger, J.-R.; Landois, P.; Mikolasek, M.; Contreras, S.; Sauvajol, J.-L.; Dujardin, E.; Zahab, A.-A. Reversible optical doping of graphene, *Sci. Rep.;* **2013**, 3, 2355.

[11] Krauss, B.; Lohmann, T.; Chae, D.-H.; Haluska, M.; von Klitzing, K.; Smet, J.H. Laser-induced disassembly of a graphene single crystal into a nanocrystalline network, *Phys.*

Rev. B **2009**, 79, 165428

[12] Han, G.H.; Chae, S.J.; Kim, E.S.; Güneş, F.; Lee, I.H.; Lee, S.W.; Lee, S.Y.; Lim, S.C.; Jeong, H.K.; Jeong, M.S.; Lee, Y.H.; Laser Thinning for Monolayer Graphene Formation: Heat Sink and Interference Effect, *ACS Nano* **2011**, 5, 263–268.

[13] Piazzi, M.; Croin, L.; Vittone, E.; Amato, G. Laser-induced etching of few-layer graphene synthesized by Rapid-Chemical Vapour Deposition on Cu thin films, *SpringerPlus* **2012**, 1: 52.

[14] Chen, S.; Ji, H.; Chou, H.; Li, Q.; Li, H.; Suk, J. W.; Piner, R.; Liao, L.; Cai, W.; Ruoff, R. S. Millimeter-Size Single-Crystal Graphene by Suppressing Evaporative Loss of Cu During Low Pressure Chemical Vapor Deposition, *Adv. Mater;* **2013**, 25 (14), 2062-2065.

[15] Reina, A.; Jia, X.; Ho, J.; Nezich, D.; Son, H.; Bulovic, V.; Dresselhaus, M.S.; Kong, J. Large Area, Few-Layer Graphene Films on Arbitrary Substrates by Chemical Vapor Deposition, *Nano Lett.* 2009, 9, 30–35.

[16] Ni, Z.; Wang, Y.; Yu, T.; Shen, Z. Raman spectroscopy and imaging of graphene, *Nano Res.* **2010**, 1, 273–291.

[17] Jorio, A. Raman Spectroscopy in Graphene-Based Systems: Prototypes for Nanoscience and Nanometrology, *International Scholarly Research Notices* **2012**, e234216.

[18] Okada, S. Energetics of nanoscale graphene ribbons: Edge geometries and electronic structures. *Phys. Rev. B*, **2008**, 77, 041408.

[19] Crow E.L.; Shimizu K. *Lognormal Distributions: Theory and Applications*, CRC Press, Boca Raton **1987.**Calizo, I.; Balandin, A. A.; Bao, W.; Miao, F.; Lau, C. N. Temperature Dependence

of the Raman Spectra of Graphene and Graphene Multilayers, *Nano Lett.*, **2007**, 7, 2645-2649.

[20] Malko, D.; Neiss, C.; Viñes, F.; Görling, A. Competition for Graphene: Graphynes with Direction-Dependent Dirac Cones, *Phys. Rev. Lett.* **2012**,108, 086804.

[21] Wang, J.; Deng, S.; Liu, Z.; Liu, Z.; The rare two-dimensional materials with Dirac cones, *Natl Sci Rev* **2015**, 2, 22–39.

[22] Farjam, M. Visualizing the influence of point defects on the electronic band structure of graphene, *J. Phys.: Condens. Matter* **2014**, 26, 155502.

Figure Captions

Figure 1 a) A comparison between Raman spectra from exfoliated (top) and CVD (bottom) graphene samples. The latter is acquired by a macro-Raman tool with spot size of 100 μm. b) Enlargement of the low energy region of Raman spectra of a CVD sample acquired with a macro-tool (bottom) and a microscope with laser spot size of about 2 μm (top), which is the result of averaging ~1400 spectra from a 42 μm x 32 μm map.

Figure 2 a) and b): I_D/I_G Raman peak intensity ratio maps of the same region from CVD graphene taken at increasing laser power, 80% and 100%, respectively. c) shows the difference between the I_D/I_G intensity ratios in b) and a), [b)-a)]. Figs. d) and e) show maps from another region, taken at decreasing power, 100% and 80%, respectively; their difference [e)-d)] is shown in f). The two color bars pertain to a), b), d), e) maps and to the corresponding differences in c) and f), respectively. Scale bar is 4 μm.

Figure 3 Histograms of the I_D/I_G intensity ratio from two Raman maps taken on separate regions of a CVD graphene sample at 80% and 100% laser power levels. Inset: the same for the I_{2D}/I_G intensity ratio.

Figure 4 a) The characteristic dependence of the I_D/I_G intensity ratio vs. square root of time. Triangles and circles indicate data collected from two different sample spots displaying typical monolayer Raman features, whereas squares refer to a sample bilayer region. b) Behavior of the I_D/I_G peak ratio vs. $t^{1/2}$ (left axis) measured at four successive laser power densities (Ψ), which are represented by the colored bar chart (right axis). The slope of the linear fit of the four sets of data are shown in the inset as function of the laser power density (log-log scale). The slope, in the log-log scale, is $\kappa \approx (1.0 \pm 0.2)$.

Figure 5 Behavior of the Raman shift of the *G* peak as function of laser illumination time, at three successive laser power values.

Figure 6 The correlation between the I_D/I_G and the I_{2D}/I_G peak ratios from two graphene regions irradiated at 80% (red circles) and 100% (blue circles) power levels. The two larger markers represent the 1st, 2nd (median) and 3rd quartiles of the two clouds of data, evidencing that sample irradiation enhances the *D* peak at the expenses of the *2D* one.

Figure1
Click here to download Figure: Fig1.jpg

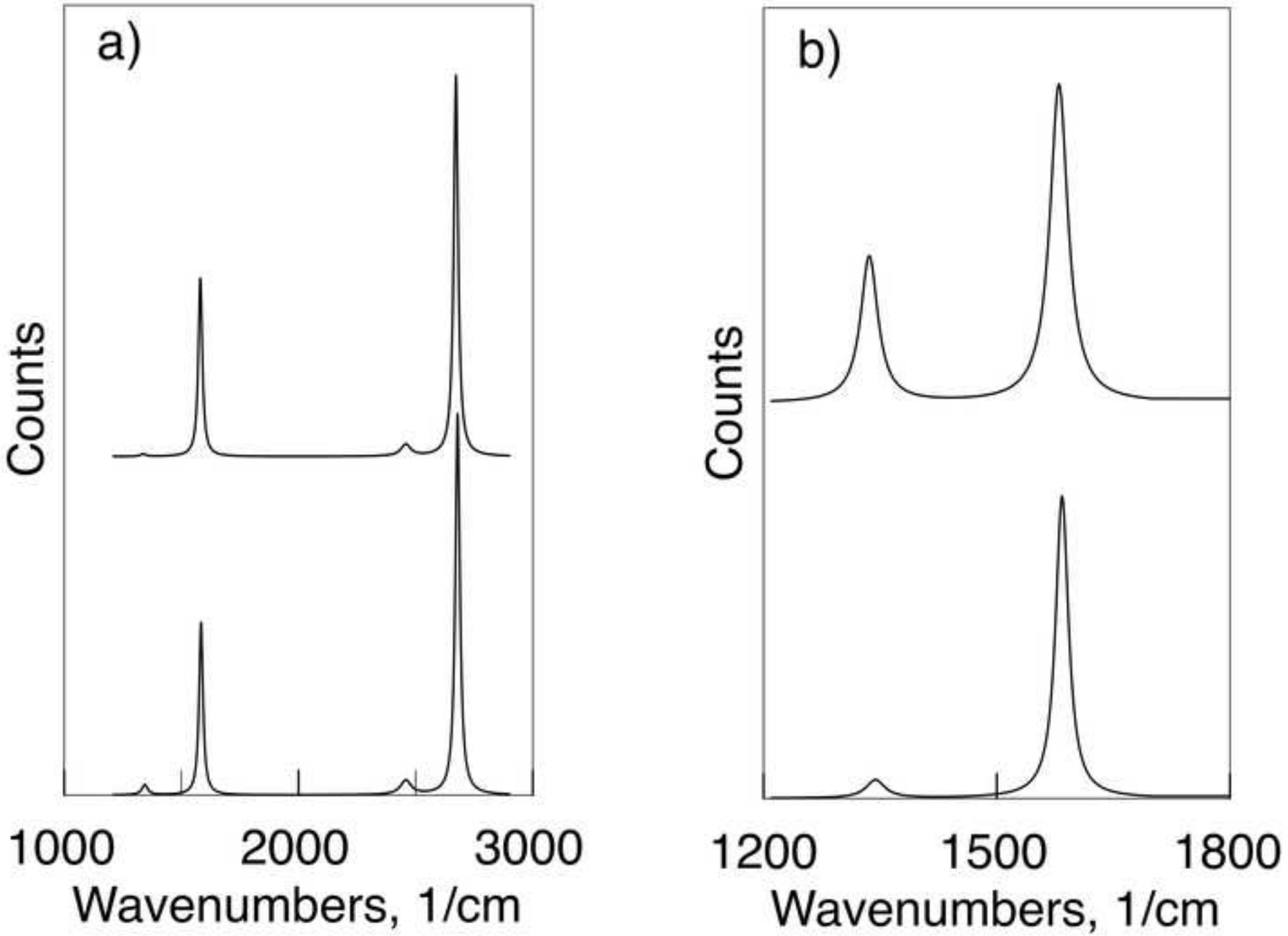

Figure2
Click here to download Figure: Fig2.jpg

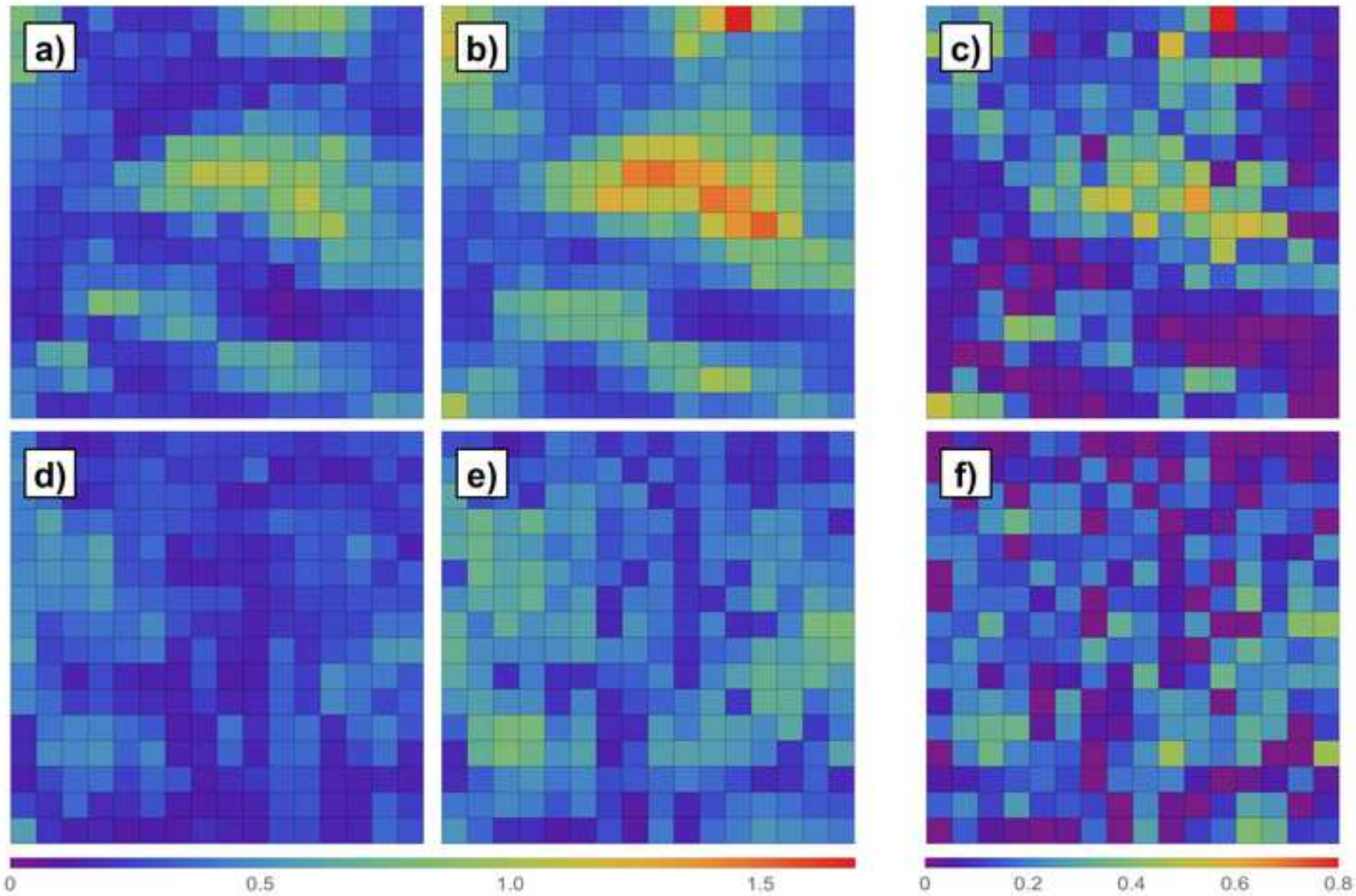

Figure3
Click here to download Figure: Fig3.jpg

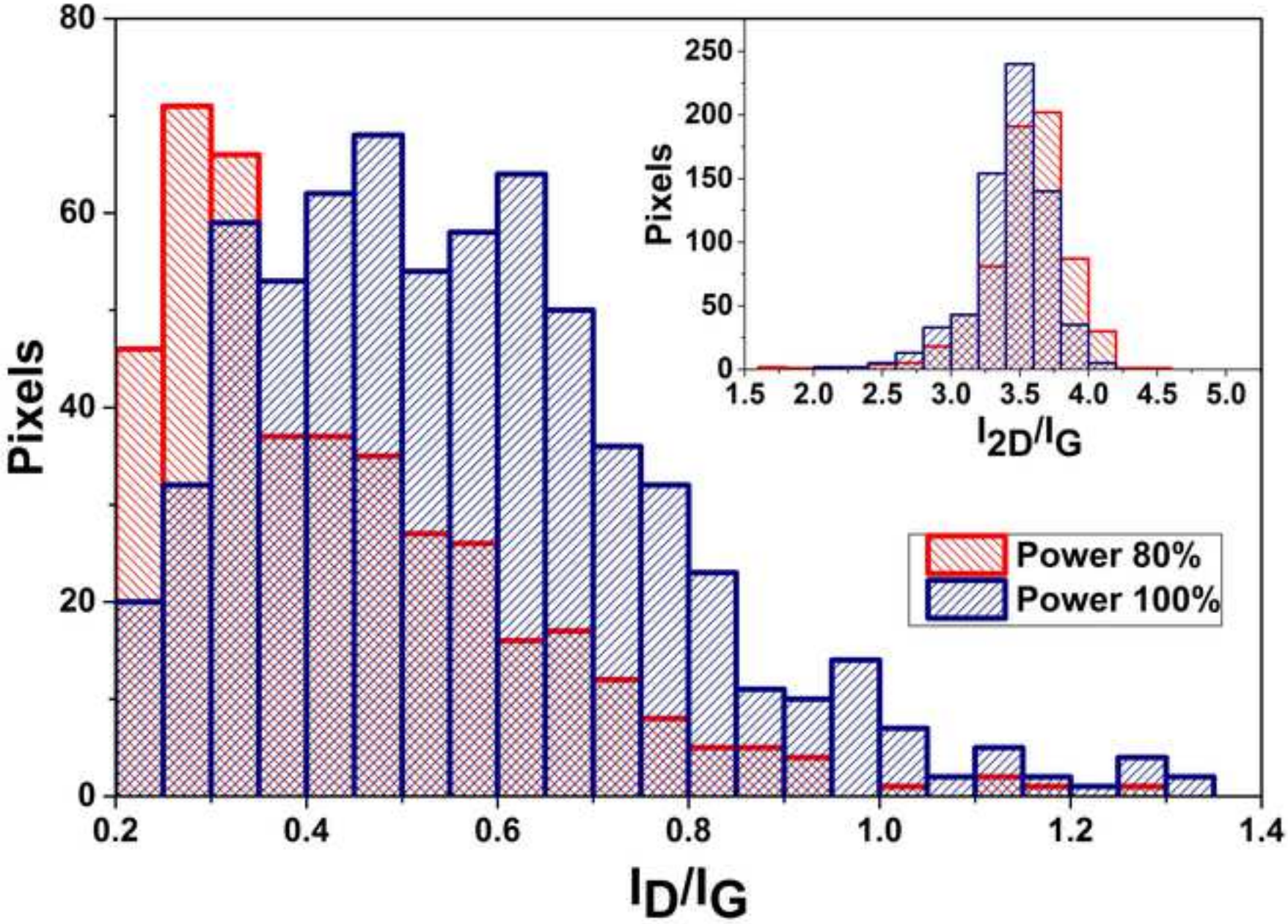

Figure4a
Click here to download Figure: Fig4a.jpg

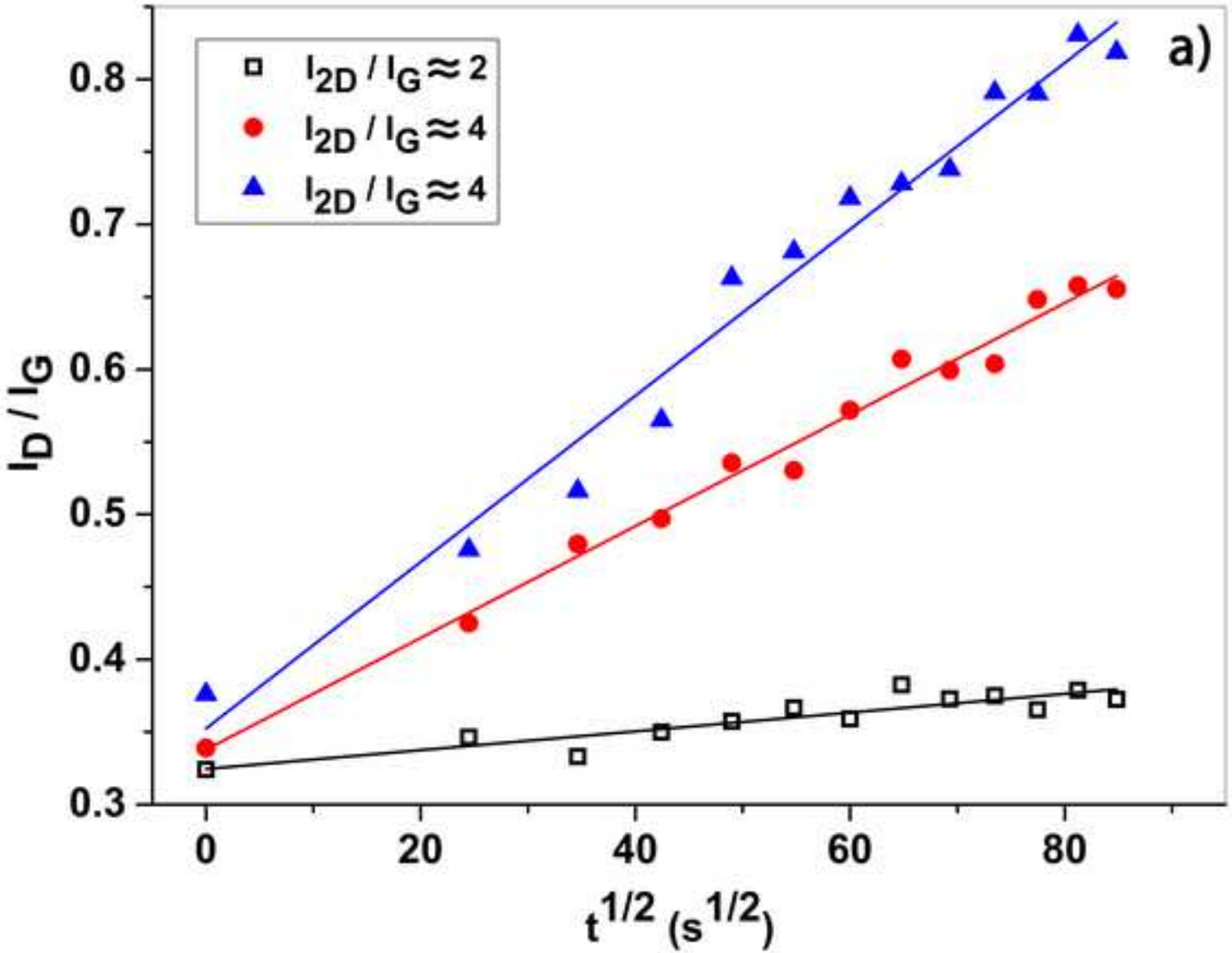

Figure4b
Click here to download Figure: Fig4b.jpg

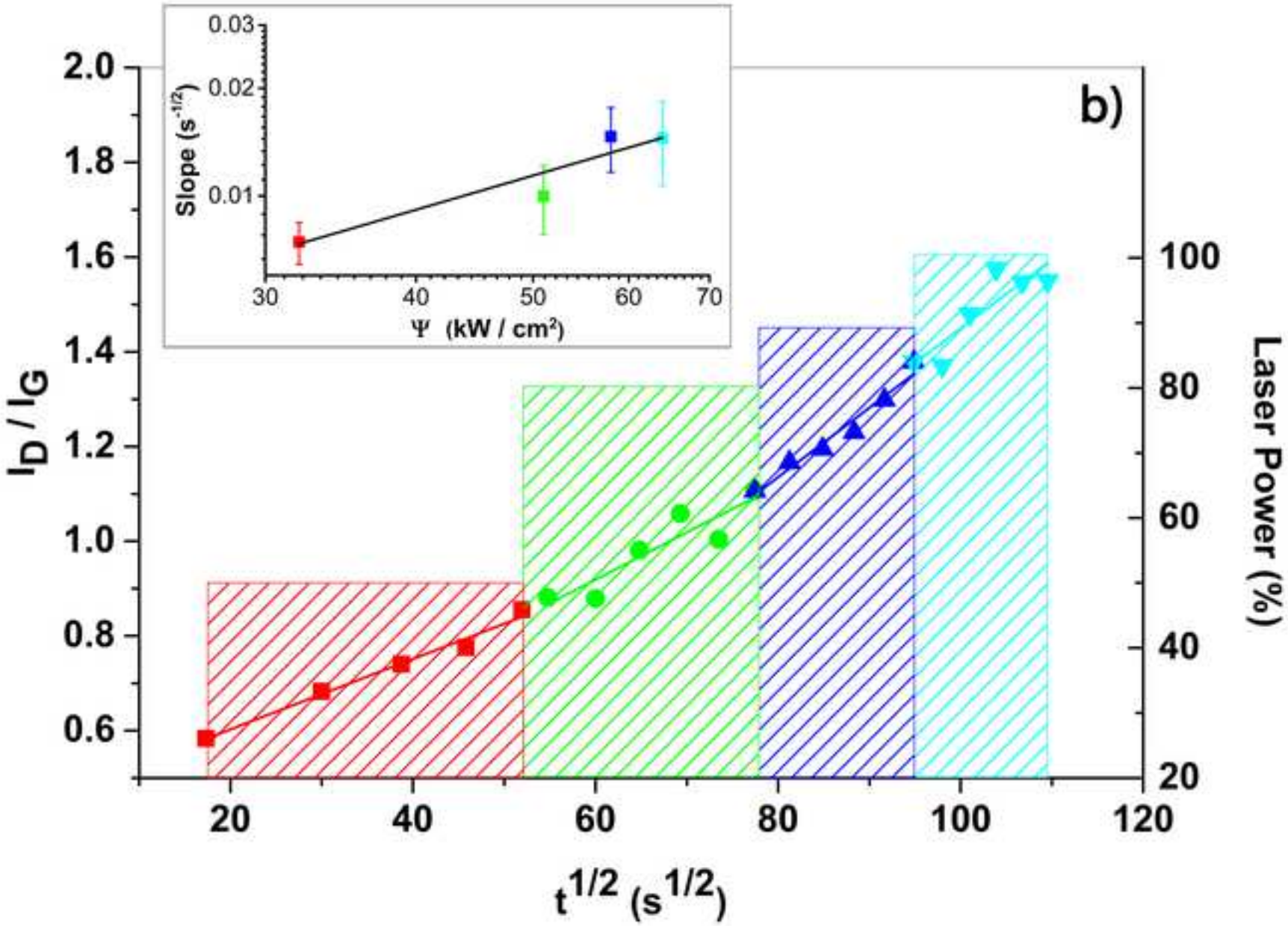

Figure5
Click here to download Figure: Fig5.jpg

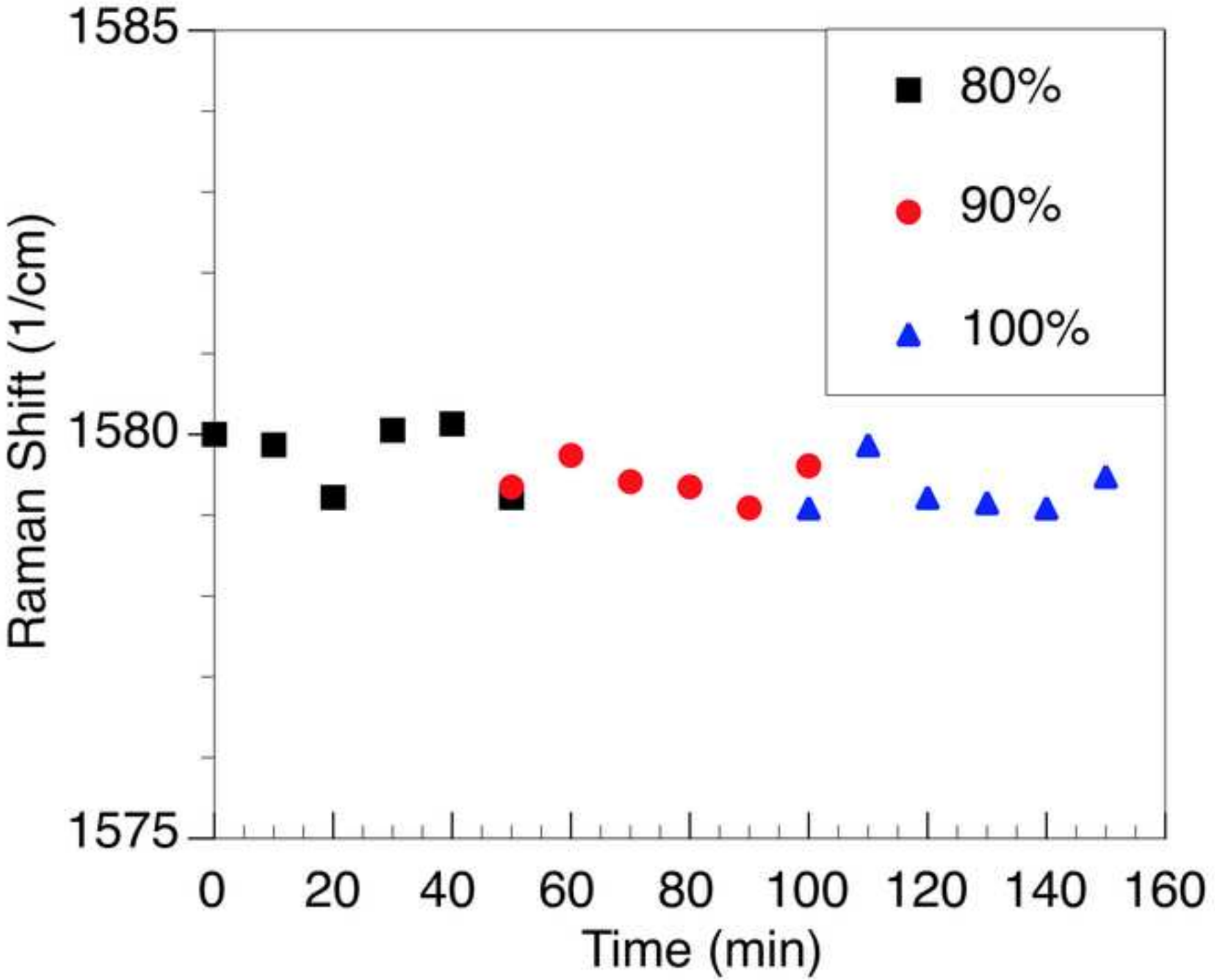

Figure6
Click here to download Figure: Fig6.jpg